in Table II, except for particle identification, are imposed, the background (highly unphysical) disappears and the remaining events appear as shown in Fig. 6. These events have particle identification incompatible with real $K\Lambda$ decays. A previous experiment[16] with similar pictures showed that only 3.7% of all true events would have particle-identification errors of this sort: a particle unequivocally called a pion which is really a proton. Furthermore, multiple remeasurements of the events are all rejected (background events tend to have shallow minima in the log of their likelihood functions, and are usually widely changed upon remeasurement), and these "marginal" events have physical features, like long lifetimes, placing them below 0.1% probability of being real. Thus the most probable conclusion of this experiment is that no real events were seen.

In Fig. 7, we show a contour map of the probability of this result as a function of the total cross sections (averaged from threshold to 1530 MeV) of the $K\Lambda$ and $K\Sigma$ reactions, $\bar{\sigma}_\Lambda/\bar{\sigma}_\Sigma$ as given by the behavior in Fig. 3. For this ratio only, we use the 10% contour (corresponds roughly to the 90% confidence level) and find the upper limits

$$\bar{\sigma}_\Lambda \leq 2.4\ \mu\text{b},$$
$$\bar{\sigma}_\Sigma \leq 2.1\ \mu\text{b}.$$

These upper limits indicate that previous estimates of these cross sections are too high. They certainly dictate a good deal of caution for the experimenter interested in obtaining a statistically significant sample of such events for phenomenological studies.

[16] L. J. Fretwell, Jr. and J. H. Mullins, Phys. Rev. **155**, 1497 (1967).

ACKNOWLEDGMENTS

We wish to thank our colleague, Dr. L. J. Fretwell, for ready exchange of information and techniques on parts of this experiment related to his work. We also acknowledge the help of the entire Cal Tech Synchrotron crew during the experimental run.

PHYSICAL REVIEW VOLUME 157, NUMBER 5 25 MAY 1967

Single and Multiple Pion Production in π^+n and π^-p Interactions at 1.7 GeV/c

T. C. Bacon,* W. J. Fickinger,* D. G. Hill, H. W. K. Hopkins,* D. K. Robinson,† and E. O. Salant*

Brookhaven National Laboratory, Upton, New York

(Received 6 January 1967)

Meson production in π^-p and π^+n interactions at 1.7 GeV/c has been studied in two bubble-chamber exposures. Combined results are presented with emphasis on single-pion production (4300 events) which is dominated by the formation of the ρ^0 meson in peripheral interactions, and on double-pion production (1100 events) which shows strong formation of the ω meson. These data are compared with the predictions of particle-exchange models, including absorption, and the effects of competing channels are discussed. Evidence for a two-pion decay mode of the ω is examined quantitatively. Processes with higher meson multiplicities are described.

I. INTRODUCTION

PION production in pion-nucleon interactions at 1.7 GeV/c has been studied in a bubble-chamber experiment. The following reactions have been analyzed and will be discussed in this paper:

$$\pi^-+p\to\pi^++\pi^-+n, \quad (1)$$
$$\pi^++d\to\pi^++\pi^-+p+p_s, \quad (2)$$
$$\pi^++d\to\pi^++\pi^-+\pi^0+p+p_s, \quad (3)$$
$$\pi^++d\to\pi^++\pi^-+\pi^++p+n, \quad (4)$$
$$\pi^++d\to\pi^++\pi^-+\pi^++d, \quad (5)$$
$$\pi^++d\to\pi^++\pi^-+\pi^++\pi^-+p+p_s, \quad (6)$$
$$\pi^++d\to\pi^++\pi^-+\pi^++\pi^-+\pi^0+p+p_s. \quad (7)$$

Reactions (1) and (2), which are charge-symmetric, are dominated by ρ^0 production, and reaction (3) by ω production. The characteristics of the production and decay processes for these resonances will be discussed. Reactions (4) and (6) take place principally through production of the $N^*(1238)$ isobar.

The symbol p_s in reactions (2), (3), (6), and (7) indicates that events were selected in which the pion interacted with the neutron in the deuteron, leaving a spectator proton.

II. THE EXPOSURES

The π^-p reactions were produced in the Brookhaven National Laboratory 20-in. hydrogen bubble chamber, exposed at the AGS to a negative beam of momentum 1.7 GeV/c. Since at this momentum the negative beam was almost entirely composed of pions, momentum

* Present address: Vanderbilt University, Nashville, Tennessee.
† Present address: Western Reserve University, Cleveland, Ohio.

analysis only was used. Momentum resolution was approximately ±0.5%. Contamination from muons and electrons was estimated to be 7±4% from the beam characteristics. Sixty thousand pictures were taken with 20–25 tracks per picture. The bubble density was kept low (~12 bubbles/cm) so that the chamber's excellent ionization discrimination could be employed in identifying the charged particles.

The π^+ exposure in the deuterium-filled chamber used the same beam transport system as the π^- hydrogen exposure with the addition of beam separators. Lepton contamination was again estimated to be about 7%. Proton contamination was negligible. A total of 120 000 pictures were taken, of which 60 000 were used for this experiment.

III. SCANNING AND MEASURING

In both the π^- and the π^+ exposures, events were selected in a small fiducial volume placed well upstream corresponding to about one-fourth of the total chamber.

A principal objective of the experiment was a detailed study of the dipion mass spectrum in the region of the ρ^0 mass with as much precision as the 20-in. bubble chamber would permit. The small scanning volume provided long secondary tracks for accurate measurements and reliable bubble density determinations. The resulting resolution function for the $\pi^+\pi^-$ fitted effective mass is shown for three mass regions in Fig. 1. The resolution function has a full width at half-maximum of about 12 MeV in the ρ mass region.

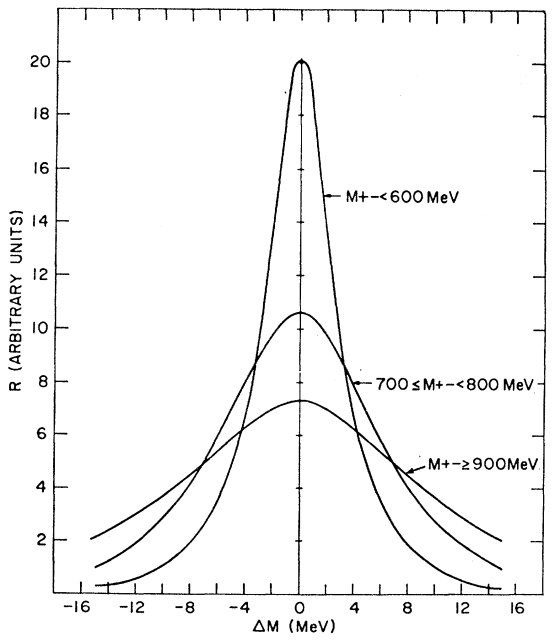

FIG. 1. Experimental resolution of the measured $\pi^+\pi^-$ effective mass for three mass regions.

In the π^- experiment, all two-pronged events within the fiducial volume were measured with the exception of those in which, at the scanning stage, the positive secondary was identified unambiguously as a proton by its ionization and curvature. To check that this scanning criterion did not eliminate events with positive pions, every two-pronged event within the fiducial volume was measured on two rolls of film (~5% of the total), and the events were identified by kinematic fitting and examination of ionization in the usual manner. No events were found in which the original scanner had mistakenly identified a positive pion as a proton. Thus it appears that good π^+ events were not accidentally eliminated at the scanning table. The π^-p events were measured on digitized projectors and microscopes, and reconstructed with the Brookhaven TRED program and kinematically fitted with GUTS.

In the π^+ exposure 42 000 frames were scanned for all nonstrange events with three or more outgoing prongs, and an additional 20 000 frames were scanned for four-prong events only. The film was scanned on measuring machines so that each event was measured as soon as it was found. Events were reconstructed with TRED and fitted with KICK.

To eliminate kinematic ambiguities, secondary tracks in both parts of the experiment were identified by ionization either visually or, if necessary, by gap counting on the film. The χ^2 and missing-mass distributions for fitted events agreed with expectation.

IV. SPECTATOR PROTONS

The reaction products of the π^+n events are accompanied by a spectator proton, either seen (even-pronged events) or unseen (odd-pronged events). When there

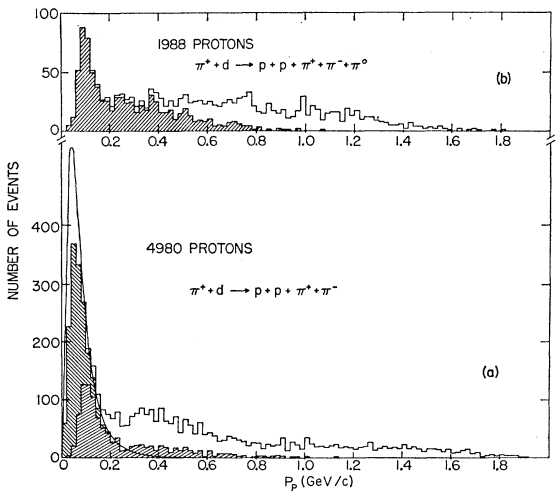

FIG. 2. Distribution of proton momenta in the laboratory system. The shaded regions correspond to the slower, or spectator, protons. (a) $\pi^+d \rightarrow pp\pi^+\pi^-$. Visible and invisible spectators are distinguished by two types of shading. (b) $\pi^+d \rightarrow pp\pi^+\pi^-\pi^0$. Only visible spectators can be shown.

are two protons in the final state we define the proton of lower laboratory momentum to be the "spectator proton" and the other to be the "recoil proton." A histogram of the momenta of both protons from reaction (2) is shown in Fig. 2(a) and from reaction (3) in Fig. 2(b). In Fig. 2(a) both three-pronged events (fitted spectators in one-constraint fits) and four-pronged events (measured spectators in four-constraint fits) have been included. Figure 2(b) includes only four-pronged events. The shaded regions correspond to the slower, or spectator, protons. In Fig. 2(a), the visible and invisible spectator protons have been shaded separately. The curve on the histogram represents the momentum distribution of the proton in the deuteron as predicted by the Hulthén wave function. This curve has been normalized to the shaded area. Since the curve and the shaded region have the same shape below 0.3 GeV/c, the impulse approximation may be considered to be valid in that region.

It should be noted that the calculated effective masses and decay angles of the multipion system are independent of the choice of spectator proton. In the impulse approximation, the square of the four-momentum transfer to the recoil proton is also independent of that choice.

In order that we may consider the neutron as a free target, we shall discuss only those events in which the spectator momentum is less than 0.2 GeV/c in the laboratory system. This limitation restricts the π^+n center-of-mass energies to the range 1.85–2.15 GeV.

The three-pronged events which are candidates for the reaction $\pi^+d \to \pi^+\pi^-\pi^0pp$ cannot be analyzed kinematically in the usual way because the momenta of both the π^0 and the invisible spectator proton are not known. Since the momenta of the spectator protons are small, and their kinetic energies negligible, these events were analyzed by introducing a dummy proton with fixed momentum ($p=20$ MeV/c, $dp/p=1.3$) in random directions. That this technique allows a reasonably accurate determination of the π^0 vector momentum is shown by the resulting $\pi^+\pi^-\pi^0$ effective-mass spectrum of Fig. 14 where three- and four-pronged events are shown separately. The calculated uncertainties in the three-pion effective masses are consistent with the observed broadening of the ω peaks in both histograms. Consequently 590 three-pronged events have been added to the 554 four-pronged events of reaction (3) and will be included in our discussion of the ω resonance (except for our determination of the ω mass and width).

V. CROSS SECTIONS

Partial cross sections measured in this experiment are listed in the last column of Tables I, II, and III. The π^-p cross sections have been determined from a count of beam tracks in a small sample of the film. They are based on a hydrogen density of 0.0586 g/cm^3. The π^+n and π^+p cross sections, determined by a track count in all the films, are based on a deuterium density of 0.1376 g/cm^3. To obtain the cross sections for the reaction with a free nucleon in deuterium, we have applied a correction of 8% for the shadowing of one nucleon by the other.[1] Table I also lists the π^-p partial cross sections at lower momenta obtained from our earlier experiments.[2,3]

Partial cross sections for specific resonant channels are listed in Table IV. These cross sections have been determined from least-squares fits to the experimental data of Breit-Wigner resonance curves and suitable phase-space backgrounds.

TABLE I. π^-p reactions at 1.08-, 1.23-, 1.38-, and 1.71-GeV/c incident pion momenta. Partial cross sections in mb.

Reaction	σ(1.08)	σ(1.23)	σ(1.38)	σ(1.71)
$\pi^-p \to \pi^-p$	25.1±3.0	14.6±0.8	15.0±0.2	10.4±0.6
$\pi^-p \to \pi^-p\pi^0$	6.5±0.5	4.3±0.3	4.3±0.2	5.8±0.4
$\pi^-p \to \pi^+n\pi^-$	10.6±0.6	7.3±0.6	7.4±0.2	7.4±0.5
$\pi^-p \to \pi^-p$+more than one neutral	0.2±0.1	0.8±0.1	1.0±0.1	1.3±0.2
$\pi^-p \to \pi^-\pi^+$+more than one neutral	0.8±0.2	3.1±0.5	3.7±0.2	4.6±0.4

TABLE II. π^+n reactions obtained from π^+d reactions at 1.68-GeV/c incident pion momentum. These cross sections have been corrected by the Glauber method for shading of the neutron by the proton. Partial cross sections in mb.

Reaction	σ(1.68)
$\pi^+n \to \pi^-\pi^+p$	6.6 ±0.3
$\pi^+h \to \pi^-\pi^+\pi^0p$	5.0 ±0.3
$\pi^+n \to \pi^-\pi^+p$+more than one neutral	0.7 ±0.1
$\pi^+n \to \pi^-\pi^+\pi^-\pi^+p$	0.22±0.04
$\pi^+n \to \pi^-\pi^+\pi^-\pi^+\pi^0p$	0.04±0.02

TABLE III. π^+d reactions at 1.68-GeV/c incident pion momentum. Partial cross sections in mb.

Reaction	σ(1.68)
$\pi^+d \to \pi^-\pi^+\pi^+np$	3.27±0.14
$\pi^+d \to \pi^-\pi^+\pi^+d$	0.07±0.02

TABLE IV. Resonance production cross sections in mb at 1.08, 1.38, and 1.71 GeV/c.

Final state	σ(1.08)	σ(1.38)	σ(1.71)
$N\rho^0$	Negligible	4.4±0.3	4.7 ±0.2
$N^*_{3/2\pi}$	3.6±0.6	1.4±0.2	1.0 ±0.3
$p\omega_{+-0}$			1.8 ±0.2
$p\eta_{+-0}$			0.15±0.04
$p\eta^*_{+-+-0}(960)$			<0.025

[1] R. Glauber, Phys. Rev. **100**, 242 (1955).
[2] E. Pickup, D. K. Robinson, E. O. Salant, F. Ayer, and B. A. Munir, Phys. Rev. **132**, 1819 (1963).
[3] E. Pickup, D. K. Robinson, and E. O. Salant, Phys. Rev. Letters **7**, 192 (1961); **7**, 472(E) (1961).

VI. SINGLE-PION PRODUCTION

In this section we discuss reactions (1) and (2) and, assuming charge symmetry, combine the data. Our measured cross sections and distributions from the π^-p and π^+n experiments are all consistent with this assumption. It is clear from Table IV that at beam momenta between 1 and 2 GeV/c, the dominant processes in reactions (1) and (2) are

$$\pi^-+p\rightarrow\pi^++N_{3/2}{}^{*-}\searrow\pi^-+n, \tag{1a}$$

$$\pi^++n\rightarrow\pi^-+N_{3/2}{}^{*++}\searrow\pi^++p, \tag{2a}$$

$$\pi^-+p\rightarrow n+\rho^0\searrow\pi^-+\pi^+, \tag{1b}$$

$$\pi^++n\rightarrow p+\rho^0\searrow\pi^-+\pi^+. \tag{2b}$$

We note that at 1.7 GeV/c ρ^0 production predominates.

Other charge states of the $\frac{3}{2}$, $\frac{3}{2}$ isobar may also be produced through the reactions

$$\pi^-+p\rightarrow\pi^-+N_{3/2}{}^{*+}\searrow\pi^++n \tag{1c}$$

and

$$\pi^++n\rightarrow\pi^++N_{3/2}{}^{*0}\searrow p+\pi^-. \tag{2c}$$

However, these states with $|I_3|=\frac{1}{2}$ are produced less strongly than the states with $|I_3|=\frac{3}{2}$, and are consequently difficult to distinguish at these energies from the kinematic reflections of the ρ meson. Similar considerations apply to the production of the higher pion-nucleon resonances, $N_{1/2}{}^*(1480)$, $N_{1/2}{}^*(1518)$, and $N_{1/2}{}^*(1688)$.

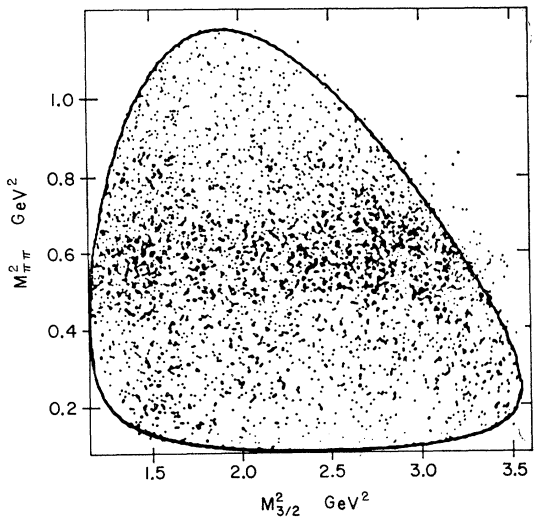

FIG. 3. Combined Dalitz plot for the reactions $\pi^-p\rightarrow\pi^+\pi^-n$ and $\pi^+n\rightarrow\pi^+\pi^-p$ (4312 events).

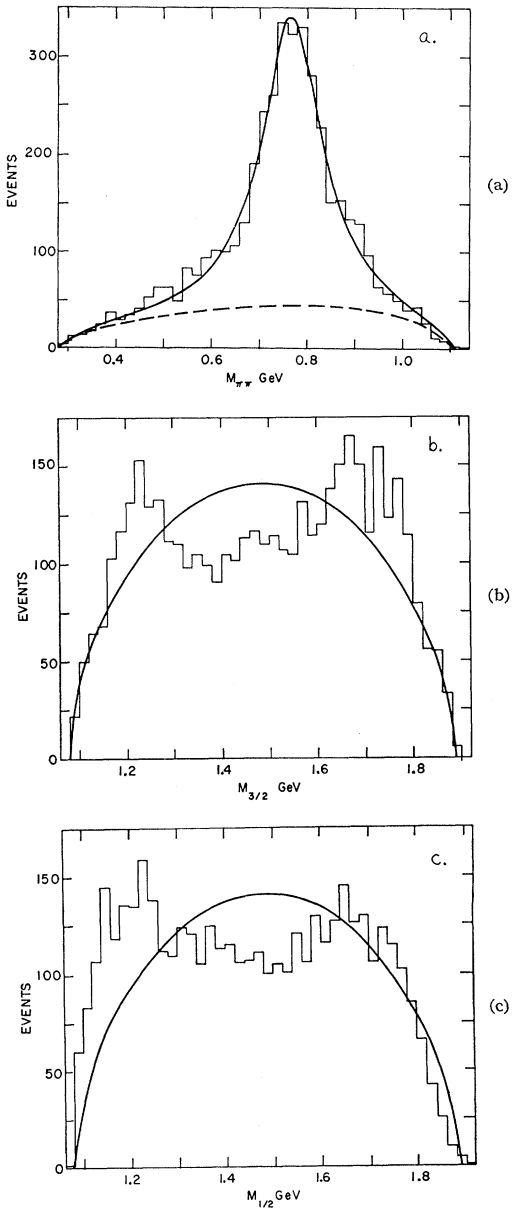

FIG. 4. Two-body effective-mass distributions for the reactions $\pi^-p\rightarrow\pi^+\pi^-n$ and $\pi^+n\rightarrow\pi^+\pi^-p$. (a) $\pi^+\pi^-$; (b) π^-n and π^+p; (c) π^+n and π^-p.

Figure 3 shows a Dalitz plot of the events from both the π^+n and the π^-p parts of the experiment, with $M^2{}_{\pi\pi}$ plotted against $M^2{}_{3/2}$. (We write $M^2{}_\tau$, where $\tau=|I_3|$.) The concentration of events about the ρ^0 mass is clearly visible. There is also a weak concentration for

$M^2_{3/2}$ in the $N^*(1238)$ region (visible outside the overlapping ρ^0 band).

The three two-body effective-mass distributions are shown in Fig. 4. The histogram in Fig. 4(a), the distribution for the dipion system, has been fitted by the least-squares method to a simple Breit-Wigner resonance plus phase-space background of the form

$$dN = A \times P(m) \times \left[B + \frac{\Gamma^2/4}{(m_0 - m)^2 + \Gamma^2/4} \right] dm,$$

where dN is the number of events in the interval between m and $m+dm$, $P(m)$ is three-body shape space for the event selection considered, and A is a normalizing parameter such that the integral of the function over m gives N, the total number of events in the histogram. Parameters of the fit are B, the constant background term; m_0, the resonance mass; and Γ, the resonance width. While this simple form with an energy-independent width Γ is not strictly correct for a broad resonance, it is used here to obtain convenient parameters from the data. In this and all our resonance fits, the experimental resolution has been folded into the calculation. The best values of the fitted parameters from this calculation are $M_\rho = 768 \pm 2$ MeV, $\Gamma_\rho = 148 \pm 8$ MeV, and $f_b = 0.321 \pm 0.017$, where f_b is the fraction of background. The fitted background is shown by the dashed curve. This simple treatment demonstrates the importance of the ρ^0 resonance in this reaction, but ignores the possible small contribution of competing intermediate channels involving the dipion and pion-nucleon systems.

Figures 4(b) and 4(c) show histograms for the $M_{3/2}(p\pi^+$ and $n\pi^-)$ and $M_{1/2}(p\pi^-$ and $n\pi^+)$ pion-nucleon systems. Both distributions show concentrations at the low and high ends of phase space. Since the reaction at this energy is dominated by ρ^0 production, we must consider the effects of kinematic reflections of p-wave $\pi\pi$ scattering on the pion-nucleon effective-mass distributions before drawing conclusions about isobar production in these reactions.

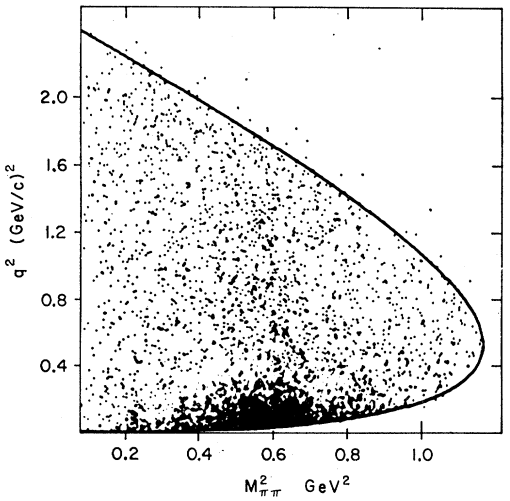

FIG. 5. Combined Chew-Low plot for the reactions $\pi^- p \to \pi^+\pi^- n$ and $\pi^+ n \to \pi^+\pi^- p$ (4312 events).

A. Production and Decay of ρ^0

Figure 5 shows a Chew-Low plot for events of single-pion production in which q^2, the square of the four-momentum transfer to the target nucleon, is plotted against $M_{\pi\pi}{}^2$. Events in the ρ^0 peak are concentrated at small q^2, characteristic of peripheral collisions, a feature observed in other experiments.

Figure 6 shows a diagram of the one-pion-exchange process for single pion production.

Figure 7 shows four distributions characteristic of ρ production and decay; (a) q^2, (b) $M_{\pi\pi}$, (c) the π-π scattering angle, $\cos\theta_{\pi\pi}$, and (d) the Treiman-Yang angle α.

1. One-Pion Exchange and Momentum Transfer Distributions

Figure 7(a) shows the distribution of momentum transfer for single-pion-production events. In agreement with earlier observations,[3,4] the peaking of the distribution at low q^2 is in qualitative accord with expectations from one-pion exchange (OPE).

For the pure OPE process of Fig. 6, the dependence of the differential production cross section on momentum transfer has been derived by Chew and Low[5] and approaches the form for small q^2,

$$\frac{\partial\sigma}{\partial q^2} \propto \frac{q^2}{(q^2 + m_\pi{}^2)^2}.$$

For ρ production in pion-nucleon collisions, although there is qualitative agreement between the predictions and the data, the absolute differential cross sections predicted by the theory are much too high. Even at low momentum transfers ($q^2 < 0.2$ (GeV/c)^2), the theoretical cross sections are almost twice as large as the experimental values. Similar discrepancies appear when the OPE predictions are compared with the

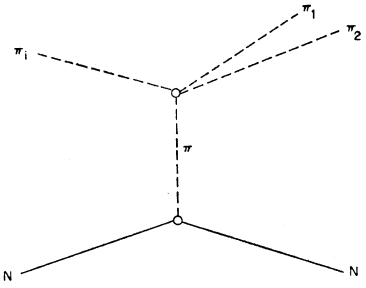

FIG. 6. Diagram of the one-pion-exchange process for single pion production.

[4] A. R. Erwin, R. March, W. D. Walker, and E. West, Phys. Rev. Letters **6**, 628 (1961).
[5] G. F. Chew and F. E. Low, Phys. Rev. **113**, 1640 (1959).

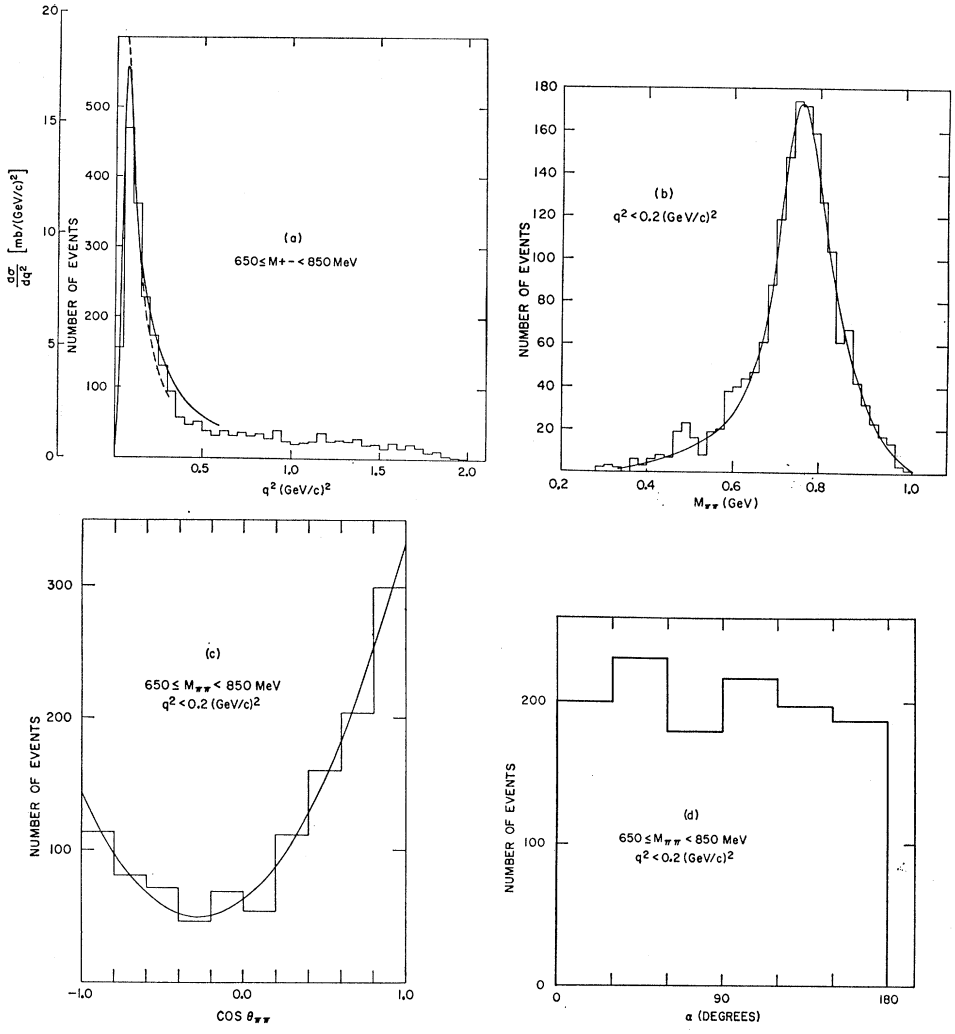

FIG. 7. Gross features of ρ^0 production. (a) Square of the invariant four-momentum transfer to the ρ^0 (2742 events); the solid curve is from a form-factor calculation; the dotted curve is from an OPE absorption calculation. (b) $\pi^+\pi^-$ effective mass distribution for small momentum transfer (1716 events). (c) $\pi\pi$ scattering angular distribution for ρ^0 events and $q^2<0.2$ $(\mathrm{GeV}/c)^2$ (1213 events). (d) Treiman-Yang angle for ρ^0 events at low q^2 (1213 events).

data on isobar production in pp interactions, e.g., $p+p\rightarrow N^*(1238)+n$.[6]

Much better agreement, both in π-p and p-p interactions, has been obtained by Ferrari and Selleri,[7] by taking into account off-shell scattering and introducing phenomenological pionic form factors of the nucleon. The form factor provides a sharp decrease of $\partial\sigma/\partial q^2$ with increasing q^2, in agreement with many observations. However, this approach predicts twice too large a cross section for anti-isobar production in $\bar{p}n$ interactions, $\bar{p}+d\rightarrow\bar{N}^*(1238)+p+p$,[8] where strong nucleon-antinucleon interactions in the initial and final states are to be expected.

Jackson and his collaborators[9,10] and Durand and Chiu[11] have studied the effects of initial and final-state absorptions on the OPE process; in these studies, the shape of the diffraction pattern is used to estimate the absorptive structure of the nucleon. The effect of this absorption is to suppress the lower partial waves and decrease the calculated differential cross sections at high momentum transfers, in agreement with observations of $\pi p\rightarrow\rho n$ reactions from 1.6 to 8 GeV/c.[9] This approach is less successful in dealing with vector-meson exchange as will be seen in Sec. VII.

The various theories are treated in the excellent review article by Jackson.[10] Predictions from the form-factor calculations,[12] and from absorptive OPE calculations[9,10] are shown in Fig. 7(a). Both theories show reasonable agreement with the data.

[6] W. J. Fickinger, E. Pickup, D. K. Robinson, and E. O. Salant, Phys. Rev. Letters **7**, 196 (1961).
[7] E. Ferrari and F. Selleri, Nuovo Cimento **27**, 1450 (1963).
[8] T. C. Bacon, H. W. K. Hopkins, D. K. Robinson, E. O. Salant, A. Engler, H. E. Fisk, C. M. Meltzer, and J. Westgard, Phys. Rev. **139**, B1420 (1965).
[9] K. Gottfried and J. D. Jackson, Nuovo Cimento **34**, 735 (1964).
[10] J. D. Jackson, J. T. Donohue, K. Gottfried, R. Keyser, and B. E. Y. Svensson, Phys. Rev. **139**, B428 (1965); this paper includes references to much of published experimental data. J. D. Jackson, Rev. Mod. Phys. **37**, 484 (1965).
[11] L. Durand and Y. T. Chiu, Phys. Rev. Letters **14**, 329 (1965); **14**, 680(E) (1965).
[12] F. Selleri, Boulder Conference on High Energy Physics, University of Colorado, 1964, (unpublished).

2. The Dipion Mass Distribution

The histogram of Fig. 7(b) shows the effective mass plot of the two pions for $q^2<0.2$ (GeV/c)^2 with a fitted Breit-Wigner curve. The best-fit parameters are $M_\rho=765\pm3$ MeV, $\Gamma_\rho=154\pm10$ MeV, and $f_b=0.02\pm0.02$. We note that the background in this momentum-transfer selection is very small and, as will be determined in Sec. VI-C, isobar contamination is less than 3%.

3. The π-π Scattering Angle

Figure 7(c) shows the distribution of $\cos\theta_{\pi\pi}$ for low momentum-transfer p events [$q^2<0.2$ (GeV/c)^2 and $650\leqslant M_{\pi\pi}<850$ MeV]. The histogram exhibits the well-known asymmetry in the decay angular distribution. The curve on the histogram represents a least-squares fit to a power series in $\cos\theta_{\pi\pi}$, and has the form

$$dN=(1.0+1.5\cos\theta_{\pi\pi}+2.7\cos^2\theta_{\pi\pi})d\cos\theta_{\pi\pi}.$$

Higher powers of $\cos\theta_{\pi\pi}$ are not required for a good fit. Attempts to explain this asymmetric distribution by ρ^0-N^* interference have been unsuccessful. We note that any possible direct contamination of $N_{3/2}^*$ would be in the backward scattering angles, as may be deduced from the Dalitz plot of Fig. 3. The simplest explanation of the scattering angle distribution is that the p-wave ρ^0 interferes with an s-wave background of isospin $I=0$, since no asymmetry appears in the decay distribution of the ρ^+ and ρ^-.

Figure 8 shows the distribution of $\cos\theta$ for six $\pi\pi$ mass regions, all fitted by least squares to the power series $A_0+A_1\cos\theta+A_2\cos^2\theta$. Including higher powers of $\cos\theta$ does not significantly improve the fits. At the bottom of the figure is a plot of the asymmetry parameter, $A=(F-B)/(F+B)$, calculated for 12 $\pi\pi$ mass regions. The values of the fitted parameters A_0, A_1, and A_2 are shown as a function of the dipion mass in Fig. 9 with the Breit-Wigner mass distribution of Fig. 7(b) superimposed on the A_2 plot.

Recent attempts to explain the asymmetry in the ρ^0 decay have concentrated on interference from an $I=0$, $J=0$ meson in the same mass region as the ρ. Durand and Chiu have calculated the effects of a scalar meson

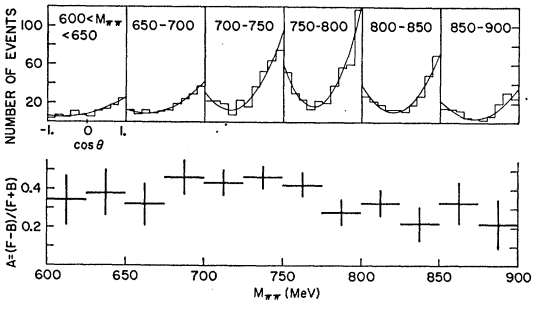

FIG. 8. The histograms show the $\pi\pi$ scattering angle for six regions of $\pi\pi$ effective mass, all for $q^2<0.2$ (GeV/c)^2. The $\pi\pi$ scattering asymmetry parameter is shown for 12 mass regions.

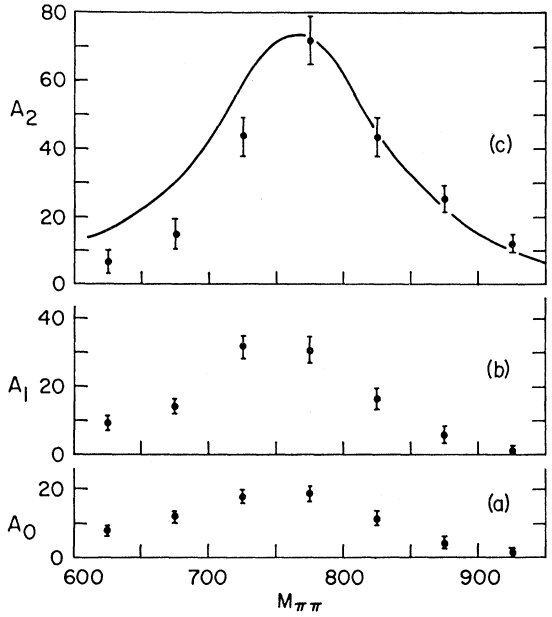

FIG. 9. Plots of the fitted coefficients of the expression $A_0+A_1\cos\theta+A_2\cos^2\theta$ for $\pi\pi$ scattering as a function of $\pi\pi$ effective mass. The curve on the A_2 plot is a Breit-Wigner fit to the ρ^0.

(ϵ_0) on the π-π scattering, using their absorption model of ρ production through OPE.[11] These calculations show that interference of the ρ with a scalar meson with a mass of ~700 MeV would be consistent with the π-π scattering distribution. A peak about 700 MeV in the neutral multipion mass spectrum reported by Feldman *et al.*[13] is a candidate for the resonance. Also, in an experiment similar to ours at 3.0 GeV, the Penn-Saclay collaboration[14] has observed some indication of a peak around 730 MeV in the $\pi^+\pi^-$ state. To observe this peak against the large background of ρ meson production, these authors have selected events with low momentum transfer to the π-π system and $\pi\pi$ scattering angles near 90°, where the amplitude for a pure p-wave resonance is zero. In a similar selection of our data there is some indication of a shift of the peak toward a lower mass when $\cos\theta$ is restricted to small values (as observed by the Penn-Saclay collaboration), but the trend is not statistically significant. However, we note that the A_2 distribution of Fig. 9 is depleted at low energies relative to the Breit-Wigner mass distribution and peaks at 780 MeV. The A_0 distribution peaks at 740 MeV. These data are thus consistent with an s-wave resonance superimposed on the p-wave ρ^0, although statistics are insufficient to allow any definite conclusions. Also, effects of absorption processes on mixing the $\pi\pi$ angular momentum states have not been considered; absorption processes will cause a peaking in A_0.

[13] M. Feldman, W. Frati, J. Halpern, A. Kanofsky, M. Nussbaum, S. Richert, P. Yamin, A. Choudry, S. Devons, and J. Grunhaus, Phys. Rev. Letters **14**, 869 (1965).

[14] V. Hagopian, W. Selove, J. Alitti, J. P. Baton, and M. Neveu-René, Phys. Rev. Letters **14**, 1077 (1965).

While the scalar meson is the most attractive explanation of the $\pi\pi$ asymmetry, other possible causes must also be considered. In this experiment there is a peak in the $\pi\pi$ mass spectrum near 780 MeV which may be associated with the asymmetry [Fig. 11(b)]. This peak has been seen in several experiments[15–17] and is usually associated with the two-pion decay of the ω meson. This possibility will be discussed in Sec. VI-B. If the peak should eventually be identified as a new s- or d-wave resonance, its influence on the π-π scattering angle would be important.

4. *The Treiman-Yang Angle*

Treiman and Yang[18] have pointed out that in the exchange of a single scalar meson (Fig. 6), the production and decay planes are uncorrelated. As a consequence, the distribution in a suitably defined angle α must be isotropic for a single scalar-meson-exchange process, and all cross sections must be independent of α. In this experiment α is defined in the dipion rest frame by

$$\cos\alpha=(\hat{\pi}_e\times\hat{N}_{\text{in}})\cdot(\hat{\pi}_e\times\hat{N}_{\text{out}}),$$

where $\hat{\pi}_e$, $\hat{N}_{\text{in}}$, and $\hat{N}_{\text{out}}$ are unit vectors in the direction of the exchanged pion, the target nucleon, and the outgoing nucleon, respectively.

Figure 7(d) shows the distribution of α for the low momentum transfer events in the ρ mass region. The distribution is isotropic within statistics and is thus consistent with OPE. However, it has been observed[19–21] that there is a correlation between α and $\cos\theta_{\pi\pi}$ which is forbidden by the pure OPE model and by the form factor OPE model.

Figure 10 shows the correlation between $\cos\theta_{\pi\pi}$ and α for our events. The data have been divided into two $M_{\pi\pi}$ regions, (the two halves of the ρ peak), and into two q^2 regions to isolate any effects of the 780-MeV peak from the ρ sample. The data for the low momentum transfers [Figs. 10(a) and 10(b)] show strong correlations between $\cos\theta_{\pi\pi}$ and α. We note that the asymmetry in $\cos\theta_{\pi\pi}$ is strongly associated with the events with $\alpha<90°$, an effect which persists in experiments performed over a wide range of incident pion momenta (1.4 GeV/c,[19] 2.7–3.0 GeV/c,[20] and 4.0 GeV/c[21]).

Durand and Chiu[11] have calculated correlations between $\cos\theta_{\pi\pi}$ and α from their absorptive OPE model, including the effects of a scalar dipion at 700 MeV/c to account for the asymmetry in $\cos\theta_{\pi\pi}$. Their calculated distributions are in qualitative agreement with our measurements.

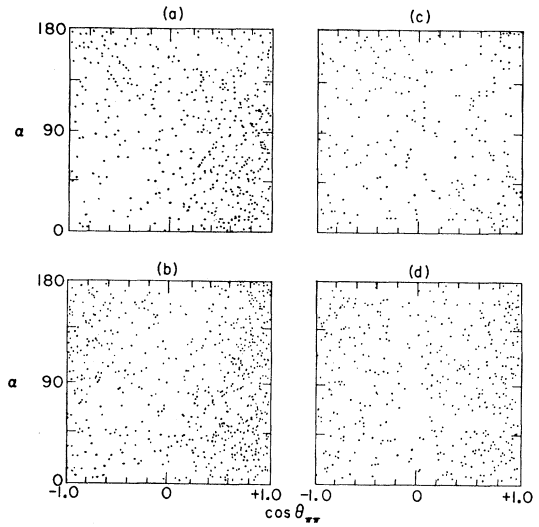

FIG. 10. Correlations between the $\pi\pi$ scattering angle and the Treiman-Yang angle for the regions: (a) $q^2<0.2$ (GeV/c)^2, $650\leq M_{\pi\pi}<750$ MeV; (b) $q^2<0.2$ (GeV/c)^2, $750\leq M_{\pi\pi}<850$ MeV; (c) $0.2\leq q^2<0.7$ (GeV/c)^2, $650\leq M_{\pi\pi}<750$ MeV; (d) $0.2\leq q^2<0.7$ (GeV/c)^2, $750\leq M_{\pi\pi}<850$ MeV.

B. Possible Two-Pion Decay of the ω Meson

The results of the π^+d portion of the experiment confirm our report[15] from the π^-p work of a peak in the π-π mass distribution near the ω mass at intermediate momentum transfers. The combined dipion mass plots are shown for three selections of the dipion production angle in Fig. 11, with events from the π^+d experiment shaded.

A strong peak near 780 MeV appears only in the intermediate production-angle selection. Since the peak is present in both our π^-p experiment (two-pronged events) and the π^+d experiment (three- and four-pronged events) with their different topologies and kinematics, it cannot be explained readily as a bias in event detection or processing. Nor can it be associated with the isobars in any simple kinematic way, although interference effects cannot be excluded. However, the appearance of this peak at the same mass in a K^-p experiment[16] and in another π^-p experiment at 2.75 GeV/c[17] argues strongly against this possibility.

It is reasonable to conclude that this peak represents a neutral state which is produced in nonperipheral interactions and decays into two pions. As mentioned in Sec. VI-A, the asymmetry in the $\pi\pi$ scattering distribution in the ρ region may be explained in terms of interference with an $I=0$ dipion state of positive parity, and has been associated with the scalar ϵ^0. The possibility that the 780-MeV peak represents such a state

[15] W. J. Fickinger, D. K. Robinson, and E. O. Salant, Phys. Rev. Letters **10**, 457 (1963).
[16] S. Flatté, D. Huwe, J. Murray, J. Button-Shafer, F. Solmitz, M. Stevenson, and C. Wohl, Phys. Rev. Letters **14**, 1095 (1965).
[17] Saclay-Orsay-Bari-Bologna Collaboration, Nuovo Cimento **35**, 713 (1965).
[18] S. B. Treiman and C. N. Yang, Phys. Rev. Letters **8**, 140 (1962).
[19] E. Pickup, D. K. Robinson, and E. O. Salant, Phys. Rev. Letters **9**, 170 (1962).
[20] V. Hagopian, W. Selove, J. Alitti, J. P. Baton, and M. Neveu-René, Phys. Rev. **145**, 1128 (1966).
[21] I. Derado, V. P. Kenney, J. A. Poirier, and W. D. Shephard, Phys. Rev. Letters **14**, 872 (1965).

cannot be excluded, although its production mechanism appears not to be one-pion exchange.

Since, however, the peak appears at the mass of the ω meson, it is reasonable to consider its interpretation in terms of two-pion decay of the ω meson. The possibility of stimulation of the two-pion decay channel of the ω due to electromagnetic interference between the ω and ρ^0, two states with the same spin and parity (1^-) and opposite G parity, was pointed out by Glashow[22] and discussed quantitatively by Bernstein and Feinberg.[23] Later calculations by Durand and Chiu[24] take into account production of the ρ^0 meson through one-pion exchange, and production of the ω meson through one-rho exchange, and the mixing of the two states by absorptive effects.

We have compared our data with equations provided by Dr. Chiu for forward and intermediate dipion production angles. Both the central mass of the ω meson and the branching ratio $R=\Gamma(\omega\to 2\pi)/\Gamma(\omega\to 3\pi)$ were parameters in a least-squares fit to the histograms of Figs. 11(a) and 11(b). The best fit to the intermediate production angle data in which the 780-MeV peak appears [Fig. 11(b)] requires $R=8\pm5\%$ and $M_\omega=782\pm3$ MeV. The fit to the forward production angle data [Fig. 11(a)] requires $R=0$. A simultaneous fit to both selections requires $R=2\pm1\%$. The χ^2 probability for the combined fit is less than 0.1% compared to $\sim$40% for the separate fits. Thus, the model fails to reproduce quantitatively the increase in size of the 780-MeV peak between forward and intermediate production angles. The calculated curve for the combined fit ($R=2\pm1\%$) and for the best fit at intermediate production angle (8%) are shown on Figs. 11(a) and 11(b).

As we have seen, the evidence for the OPE mechanism in ρ production is reasonably good. However, the evidence for ω production through single ρ exchange is not good, as will be discussed in Sec. VII. Thus, since one of the bases for the calculation of the ρ^0-ω interference is in disagreement with observations, the failure of the theory to reproduce the production angle dependence is not surprising.

Another explanation of the 780-MeV peak has been suggested by Ross and Shaw[25] who have pointed out that absorptive effects in ρ production may shift the apparent ρ mass to higher values at high momentum transfers. There appears to be some evidence for this effect in the data of the Yale group on ρ^+ production in the reaction $\pi^+p\to\rho^++p$ at 2.08 GeV/c.[26]

Our 780-MeV peak, requiring a branching ratio of 8% for $\Gamma(\omega\to 2\pi)/(\omega\to 3\pi)$, is larger than might be expected from ρ-ω interference alone. It is possible that the effect we observe is a combination of the Ross and Shaw mass shift with the stimulated 2π decay of the ω meson.

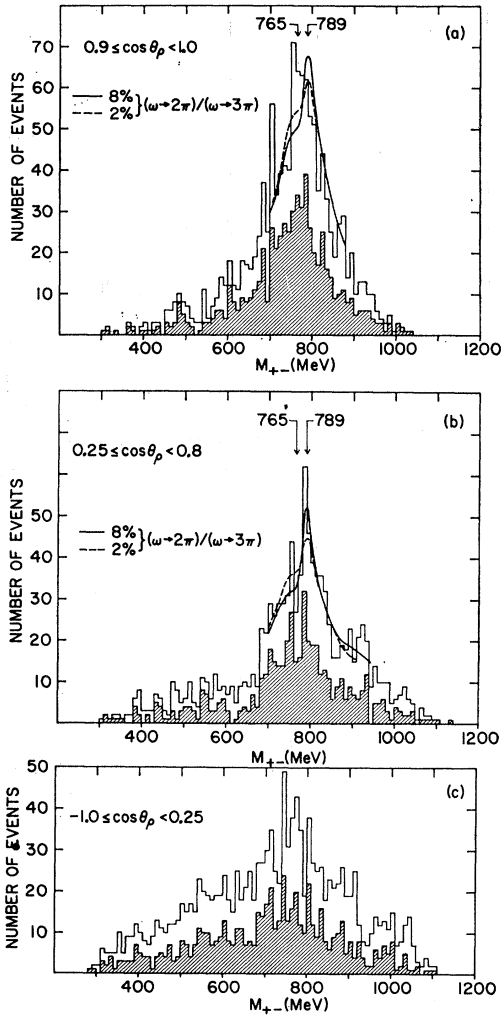

FIG. 11. Dipion mass distributions for the reactions $\pi^-p\to\pi^+\pi^-n$ and $\pi^+n\to\pi^+\pi^-p$ for three production angle cuts. The shaded events are from the π^+n sample. (a) Forward production angles, corresponding to $q^2<0.12$ (GeV/c)^2 at $M_{\pi\pi}=790$ MeV (1260 events). (b) Intermediate production angles, $0.38\leq q^2<0.68$ (GeV/c)^2 at $M_{\pi\pi}=790$ MeV (1074 events). (c) Large production angles, $q^2\geq0.68$ (GeV/c)^2 at $M_{\pi\pi}=790$ MeV (1352 events).

C. Isobar Production

As can be observed in the Dalitz plot of Fig. 3 and the effective mass plots of Fig. 4, any isobar production in this experiment is heavily masked by the ρ meson decays which tend to populate the ends of the N-π effective mass distributions. In an attempt to separate the isobars from the ρ decay background, we have used the distributions of Fig. 7 as input to a Monte Carlo calculation of "ρ reflection phase space," assuming

[22] S. Glashow, Phys. Rev. Letters **7**, 469 (1961).
[23] J. Bernstein and G. Feinberg, Nuovo Cimento **25**, 1343 (1962).
[24] L. Durand, III, and Y. T. Chiu, Phys. Rev. Letters **14**, 1039 (1965).
[25] M. H. Ross and G. L. Shaw, Phys. Rev. Letters **12**, 627 (1964).
[26] F. E. James and H. L. Kraybill, Phys. Rev. **142**, 896 (1966).

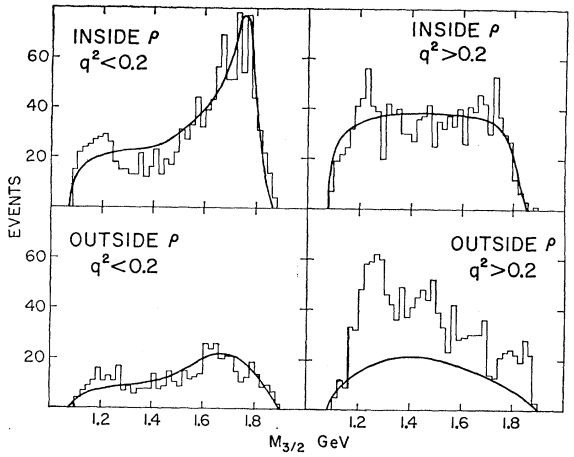

FIG. 12. Combined π^+p and π^-n effective-mass distributions for events inside the $\rho^0(650 \leq M_{\pi\pi} < 850)$ and outside, for two momentum-transfer regions. The curves are ρ^0 reflection phase space.

that the variables q^2, $M_{\pi\pi}$, $\cos\theta_{\pi\pi}$, and α are independent, as required by a model of pure ρ production through OPE. The results of the calculation are shown in Figs. 12 and 13 as curves on the distributions of the effective masses $M_{3/2}$ and $M_{1/2}$. The data have been divided into two momentum transfer regions, $q^2<0.2$ $(\mathrm{GeV}/c)^2$ and $q^2>0.2$ $(\mathrm{GeV}/c)^2$, and into the regions inside and outside the ρ $(650 \leq M_{\pi\pi} < 850$ MeV). The differences between the curves and the experimental histograms may be attributed to processes other than ρ^0 production through OPE.

There is evidence for $N^*(1238)$ production in the distribution of $M_{3/2}$ for the higher q^2 selection of Fig. 12. The peak around 1220 MeV is stronger in the selection of events which excludes the ρ mass region. The disagreement between the curve and data in this region also indicates that processes other than ρ^0 and $N_{3/2}^*$

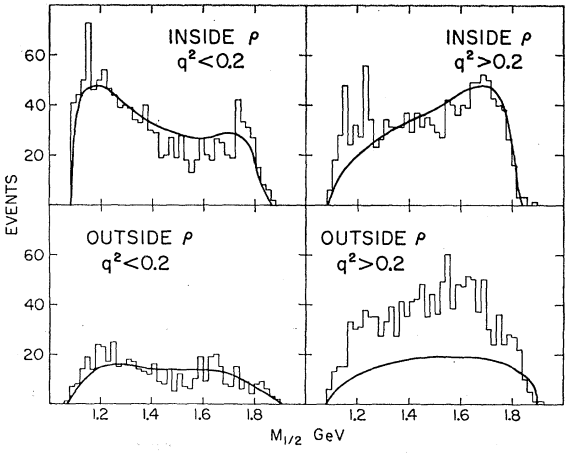

FIG. 13. Combined π^-p and π^+n effective-mass distributions for events inside the $\rho^0(650 \leq M_{\pi\pi} < 850)$ and outside, for two momentum-transfer regions. The curves are ρ^0 reflection phase space.

production are taking place. It should be noted that for the selection of events within the ρ mass region for small q^2, the curve is normalized to the data by the input properties of Fig. 7. There is little evidence for the excitation of $N^*(1238)$ or any higher isobars in the $M_{1/2}$ plot of Fig. 13.

In the low-q^2 region of Fig. 12, there is a bump around 1150 MeV for events selected within the ρ. It is difficult to attribute this accumulation to contamination of the ρ^0 sample by N^* decay, because of the low mass at which it appears. Kinematically the bump is associated with an excess of events with $\cos\theta_{\pi\pi}<0$ for $\alpha<90°$. Our input conditions to the Monte Carlo calculation assumed that the $\pi\pi$ scattering angle θ and the Treiman-Yang angle α are independent, as required by the OPE model, but it was seen in Sec. VI-A that this condition is not satisfied by the data (Fig. 10). It is difficult to determine from these data whether the discrepancy is a true $\pi\pi$ effect or an effect due to isobar interference. Selleri has suggested that interference between $N_{3/2}^*$ and the ρ^0 could shift the isobar peak to a lower pion-nucleon effective mass.[27]

From consideration of these distributions, we estimate that the cross section for producing $N_{3/2}^*$ through reaction (1a) and (2a) is 1.0 ± 0.3 mb, and that isobar contamination to the ρ^0 events of Fig. 7(b) (low q^2) is less than 3%.

VII. THE REACTION $\pi^+n \rightarrow p\pi^+\pi^-\pi^0$

A. Mass, Momentum-Transfer, and Decay Distributions

Measurements of three-pion effective-mass, four-momentum-transfer, and decay-angle distributions for four-pronged events for reaction (3) have been presented in preliminary reports.[28] The more complete data of this section agree with the material of those reports.

The three-pion effective-mass distribution is shown in Fig. 14 for both the three-pronged and four-pronged events discussed in Sec. IV. The Breit-Wigner (plus phase space) fit to the ω peak of the upper histogram (visible spectators only) gives a central mass of 789 ± 2 MeV and an intrinsic full width of 12_{-7}^{+12} MeV; a resolution of 10 MeV was included in the least-squares fitting. The area under the resonance curve gives a cross section of 1.8 ± 0.2 mb for production of ω decaying into $\pi^+\pi^-\pi^0$. The fit of the small η peak was constrained to a mass of 550 MeV and a width of 5 MeV. The area under the curve gave a cross section of 0.15 ± 0.04 mb for producing η decaying into $\pi^+\pi^-\pi^0$.

To study the production and decay properties of the

[27] F. Selleri (private communication).

[28] T. C. Bacon, H. W. K. Hopkins, D. K. Robinson, D. G. Hill, E. O. Salant, A. Engler, H. E. Fisk, C. M. Meltzer, and J. B. Westgard, in *Proceedings of the International Conference on High-Energy Physics, Dubna, 1964* (Atomizdat, Moscow, 1965), p. 532. T. C. Bacon, W. J. Fickinger, H. W. K. Hopkins, D. K. Robinson, and E. O. Salant, in *Proceedings of the Second Topical Conference on Resonant Particles* (Ohio University, Athens, Ohio, 1965), p. 129; Bull. Am. Phys. Soc. **10**, 66 (1965).

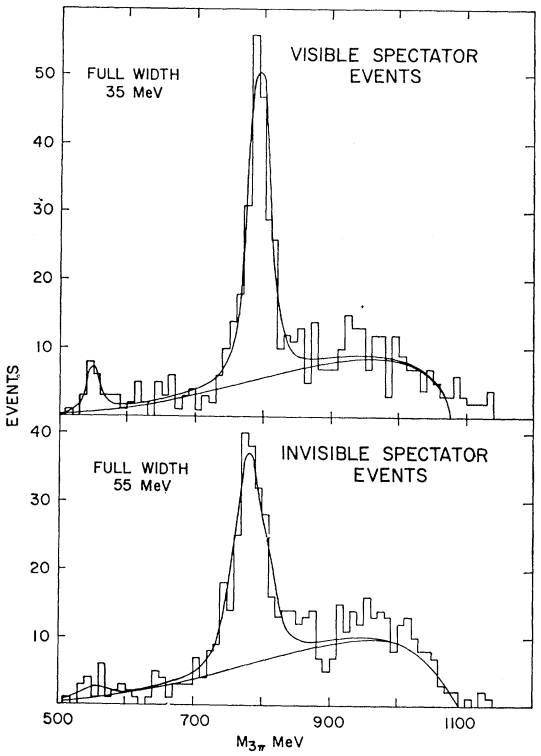

FIG. 14. $\pi^+\pi^-\pi^0$ effective-mass distributions for the reaction $\pi^+d \to pp\pi^+\pi^-\pi^0$. The curves have been calculated from least-squares fit to the data of Breit-Wigner resonance form plus phase-space background. The experimental resolution has been folded into the calculation.

ω meson, we have selected events in the mass range $750 \leqslant M_{3\pi} < 820$ MeV. From the fitted curves of Figs. 14(a) and 14(b) we estimate that there is an 18% nonresonant background included in this sample of 412 events.

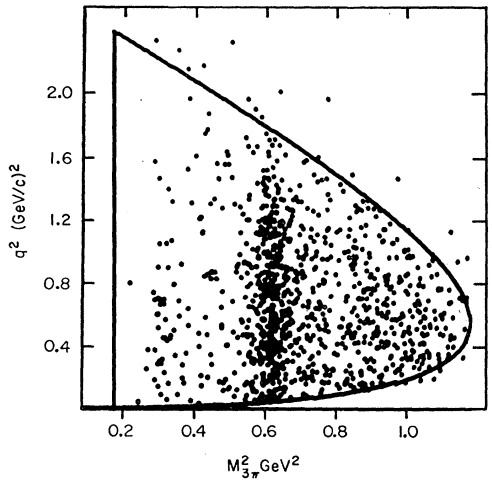

FIG. 15. Chew-Low plot for the reaction $\pi^+n \to \pi^+\pi^-\pi^0 p$ (1095 events).

Figure 15 is the Chew-Low plot of q^2 (the squared four-momentum transfer to the target nucleon) against $M_{3\pi}{}^2$. The ω meson is produced with values of q^2 extending almost to the kinematic limit. This feature is displayed again in the histogram of Fig. 18, for which the distribution in q^2 is given by the scale at the top of the figure and the distribution in the equivalent ω-production angle, θ_{prod}, is given in the bottom scale. The distribution is flat to $q^2 \sim 1$ (GeV/c)^2, and falls only as the kinematic limit is approached. Thus the ω meson is produced in central as well as peripheral collisions.[28]

Decays will be described in the ω rest system, in which the polar angle between the incident pion momentum vector and the normal to the decay plane is designated by θ, and the azimuthal angle of the normal to the decay plane about the normal to the production plane is designated by α, the Treiman-Yang angle [Fig. 16(a)]. Histograms of the θ and α distributions are shown in Fig. 17. The curves are least-squares fits to the histograms.

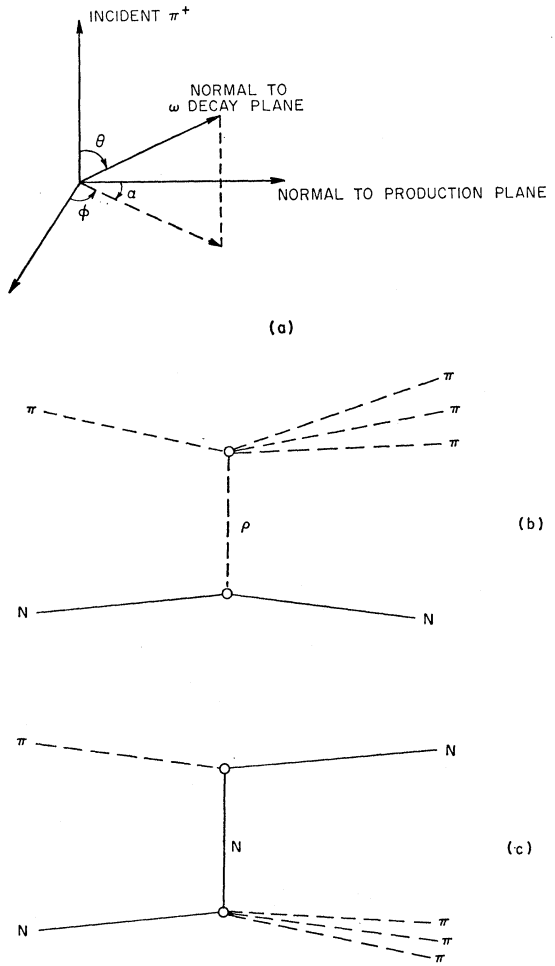

FIG. 16. (a) Vector diagram of ω decay. (b) Diagram for ω production through ρ exchange. (c) Diagram for ω production through nucleon exchange.

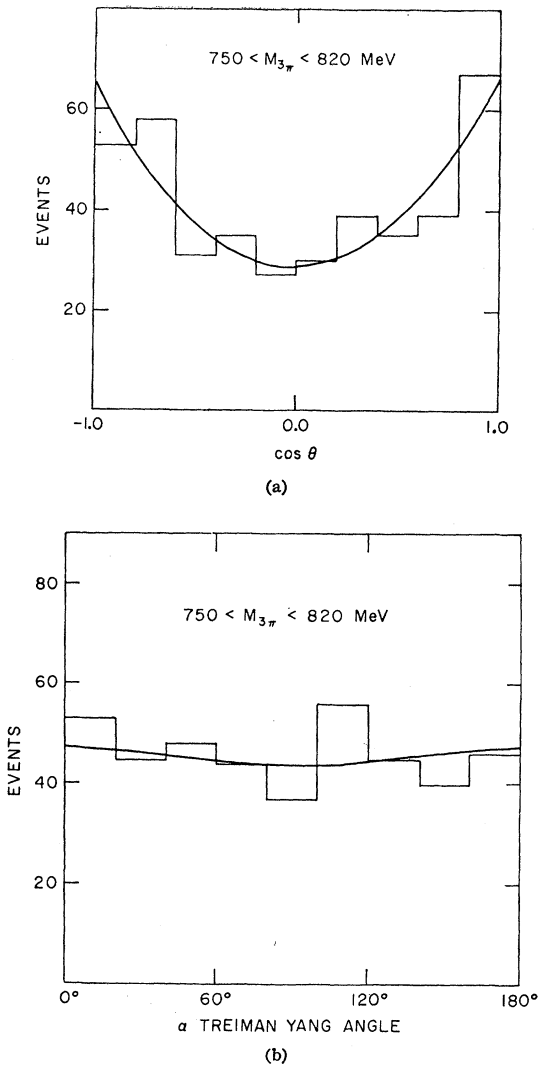

FIG. 17. Angular distributions of ω decay.

The polar distribution has been fitted to a power series in $\cos\theta$

$$W(\theta)=\text{const}\times(a+b\cos\theta+c\cos^2\theta)$$

to give $a=1.0\pm0.1$, $b=0.0\pm0.1$, $c=1.2\pm0.3$. The azimuthal distribution is uniform, given by

$$W(\alpha)=\text{const}\times[(1.00\pm0.05)+(0.02\pm0.07)\cos2\alpha].$$

The ratio of a, b, and c and the vanishing of the coefficient of the $\cos2\alpha$ term have already been noted.[28]

Gottfreid and Jackson[9] have given the relation between the decay angular distributions $W(\theta,\alpha)$ of a $J=1$ resonance and the spin-density matrix elements for the resonance's magnetic substates 0 and ±1. The dependence, written as a function of the three matrix elements $\rho_{00}(=1-2\rho_{11})$, $\rho_{1,-1}$, and $\mathrm{Re}\,\rho_{1,0}$, takes the form

$$W(\theta,\alpha)\propto[1-\rho_{00}+(3\rho_{00}-1)\cos^2\theta+\rho_{1,-1}\sin^2\theta\times\cos2\alpha-2\,\mathrm{Re}(\rho_{10})\sin2\theta\,\sin\alpha]$$

(where for the Gottfried-Jackson Φ, we substitute $\alpha=90°-\Phi$).

Averaging over the azimuthal angle gives the polar distribution, $W(\theta)=\text{const}\times[1-\rho_{00}+(3\rho_{00}-1)\cos^2\theta]$. The azimuthal distribution, obtained by averaging over the polar angle is given by $W(\alpha)=\text{const}\times(1+2\rho_{1,-1}\times\cos2\alpha)$. The remaining element can be calculated from the expression

$$\mathrm{Re}(\rho_{10})=\frac{-5}{4\sqrt{2}}\langle\sin2\theta\,\sin\alpha\rangle,$$

where $\langle\sin2\theta\,\sin\alpha\rangle$ is the average value of the function.

Values of the matrix elements determined from the angular distributions of this experiment, and averaged over all production angles are

$$\rho_{00}=0.53\pm0.04,\quad \rho_{1,-1}=0.02\pm0.04,$$
$$\mathrm{Re}(\rho_{1,0})=-0.08\pm0.02.$$

The matrix elements are shown as a function of the production angle (and q^2) in Figs. 19(a), 19(b), and 19(c).

Reaction (3) has been studied at an incident beam momentum of 1.23 GeV/c by Kraemer *et al.*,[29] and at 3.25 GeV/c by Cohn *et al.*[30] The production angular distributions (and momentum-transfer distributions) are similar at 1.23 GeV/c and in our experiment at 1.7 GeV/c. The momentum transfer distribution at 3.25 GeV/c peaks at $q^2\simeq0.2$ (GeV/c)^2 and has fallen to a quarter of the peak value at $q^2\simeq1.0$ (GeV/c)^2, in marked contrast to the flat distributions over the same range at the lower beam momenta. All three experiments show strong $\cos^2\theta$ dependence in the distributions of the polar decay angle. The distribution of the azimuthal decay angle α is practically isotropic at 1.7 GeV/c, but has strong $\cos2\alpha$ components at 3.25 GeV/c.

Thus, ω production appears to be less peripheral at 1.7 GeV/c than at 3.25 GeV/c, and the distribution of the azimuthal decay angle is more nearly isotropic at the lower momentum.

B. Comparison With Suggested Mechanisms

It has been shown that the role of a single-particle exchange mechanism and the nature of the exchanged particle can be deduced from the observed production and decay angular distributions of resonant systems.[10] However, a simple vector-meson exchange predicts a broader distribution in momentum transfer (or production angle) than is observed in a number of quasi two-

[29] R. Kraemer, L. Madansky, M. Meer, M. Nussbaum, A. Pevsner, C. Richardson, R. Strand, R. Zdanis, T. Fields, S. Orenstein, and T. Toohig, Phys. Rev. **136**, B496 (1964).
[30] H. O. Cohn, W. M. Bugg, and G. T. Condo, Phys. Letters **15**, 344 (1965).

particle reactions. In decays there is also a discrepancy: Production of the ω meson by simple ρ exchange [Fig. 16(b)] would give a $\sin^2\theta$ distribution for the polar-decay angle whereas the distribution observed in several experiments is approximately $1+\cos^2\theta$.

Attempts to remedy these defects have been made by taking into account the effects of absorption of the initial- and final-state mesons in the field of the nucleons.[10] The absorption deletes the lower partial waves, thus decreasing production at high momentum transfers, and for ω production through ρ exchange, changes the distribution of the polar decay angle from pure $\sin^2\theta$ to a strong $\cos^2\theta$ dependence.

The solid curve of Fig. 18 shows the differential production cross section predicted by this model with the experimental distribution. At very low q^2 the predicted cross section is in fair agreement with the data, but the predicted distribution is oversuppressed at high momentum transfers. Jackson has calculated the effect of adding the single-nucleon exchange process of Fig. 16(c). The result of this calculation is shown by the long-dashed curve of Fig. 18. This curve is representative of a series of calculations performed with various values of the $nn\omega$ coupling constant, and uses $G_v^2/4\pi \simeq 1.1$. The short-dashed curve has been calculated by Barmawi[31] for a 1^+ Regge pole (B-meson) exchange. Neither of these two modifications gives good agreement with the data.

Figure 19 shows the experimental values and the theoretical predictions of the spin-density matrix elements. As shown in Fig. 19(a), the absorptive ρ-exchange calculations, both with and without nucleon exchange, give values of $\rho_{0,0}$ in fair agreement with data for $q^2<0.5$ (GeV/c)^2. At higher q^2 the predicted

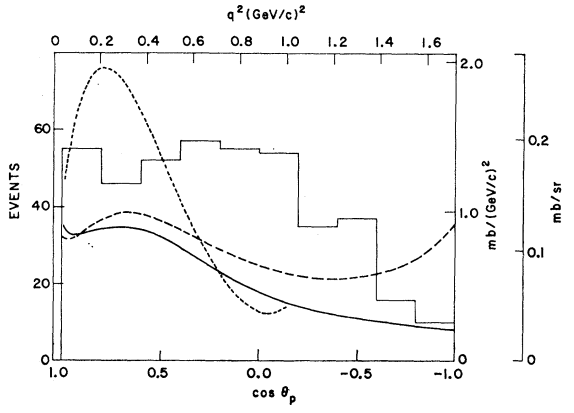

FIG. 18. Distribution in the invariant four-momentum transfer to the three-pion system for events of the reaction $\pi^+n \to \pi^+\pi^-\pi^0 p$ with $750 \leq M_{+-0} < 820$ MeV. The second abscissa scale, the cosine of the production angle, is calculated for a three-pion effective mass of 785 MeV. The solid curve represents the predictions of the ρ exchange model with absorption. The long-dashed curve represents combined nucleon and ρ exchange with absorption. The short-dashed curve shows the results of a 1^+ Regge-pole exchange without absorption.

[31] M. Barmawi, Phys. Rev. Letters **16**, 595 (1966).

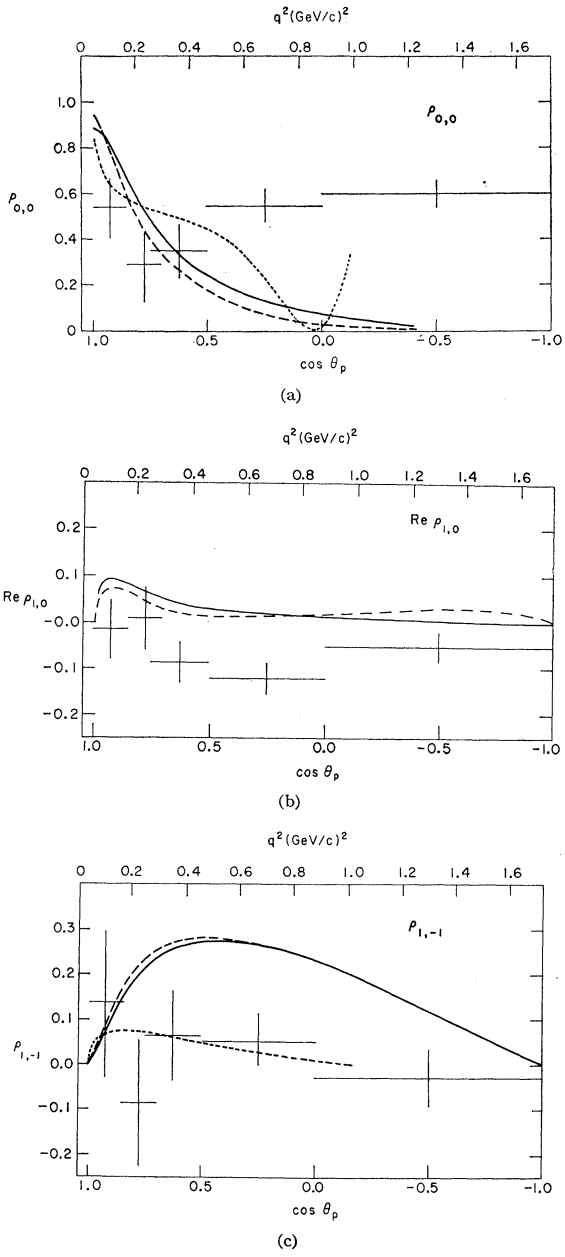

FIG. 19. The spin-density matrix elements for ω decay as a function of production angle and of momentum transfer. The meaning of the curves is the same as in Fig. 18.

values of $\rho_{0,0}$ are too low. Similar comments apply to the B-meson exchange calculation.

The uniform azimuthal distribution, given by the essentially zero values of $\rho_{1,-1}$ at all q^2 in Fig. 19(c), is not predicted by the absorptive ρ exchange, and this is not improved by the nucleon exchange. The B-exchange curve is consistent with the measurements.

In Fig. 19(b), the predictions for the coefficient of the angular correlation term Re $\rho_{1,0}$ are not in very good agreement with the measurements.

It is necessary to conclude that even with the inclusion of heavier exchanged systems, predictions based on single-particle-exchange models are inconsistent with both production and decay distributions observed in this experiment, except possibly at very low momentum transfers. However, the beam energy is sufficiently low that the models may not be strictly applicable. Obviously more knowledge about collisions at small impact parameters is needed. The non-peripheral region of a nucleon's structure provides a variety of particles for exchange, so that a one or two particle exchange mechanism may be an unrealistic simplification.

VIII. THE REACTION $\pi^+d \to \pi^+\pi^-\pi^+pn$

Figure 20 shows, for reaction (4), a scatter plot of the proton and neutron momenta in the laboratory system. The events separate naturally into a group with low-energy (spectator) neutrons and a group with low-energy (spectator) protons so that we may treat separately

$$\pi^+ + p \to \pi^+ + \pi^- + \pi^+ + p \qquad (4a)$$

and

$$\pi^+ + n \to \pi^+ + \pi^- + \pi^+ + n. \qquad (4b)$$

In order to study these reactions, we have applied a spectator momentum cutoff of 200 MeV/c. We note that events in which the proton momentum is insufficient to make a visible track in the bubble chamber are missing from the sample.

The cross section for reaction (4) corrected for unobservable low momentum protons is listed in Table I. The π^+p reaction (4a) is favored over the π^+n reaction (4b) by a factor of approximately two to one. A possible explanation of this rate is that the reactions occur through excitation of the resonant intermediate state

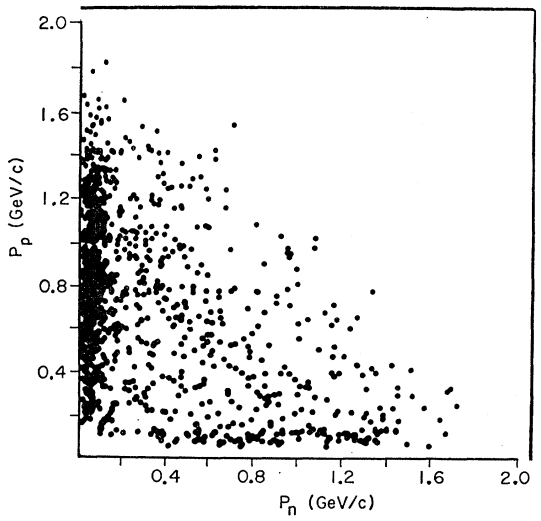

FIG. 20. Scatter plot for the reaction $\pi^+d \to \pi^+\pi^-\pi^+pn$ of the momentum of the proton against the momentum of the neutron in the laboratory system (1062 events).

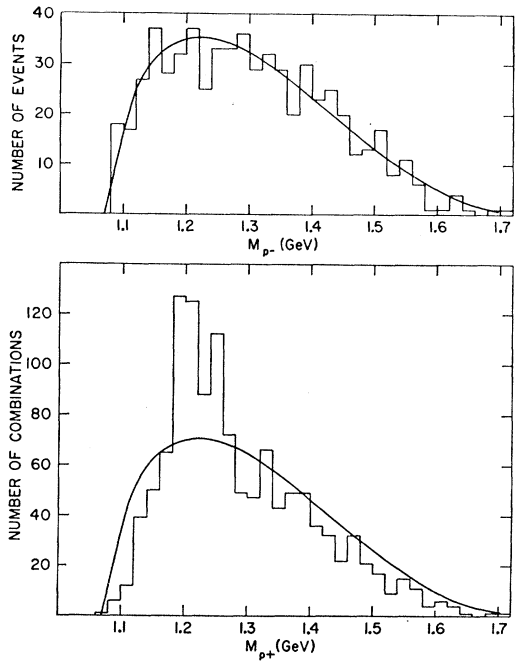

FIG. 21. Pion-nucleon effective-mass distributions from the reaction $\pi^+p \to \pi^+\pi^-\pi^+p$. The curve represents the distribution of Lorentz-invariant phase space (620 events).

$N_{3/2}$*(1924) which is close to our mean center of mass energy 2.03 GeV, thus favoring the $I=\frac{3}{2}$ π^+p state over the mixed $I=\frac{3}{2}$ and $I=\frac{1}{2}$ π^+n state.

Figure 21 shows the effective-mass distribution of the $p\pi^-$ and $p\pi^+$ systems from reaction (4a). After allowing

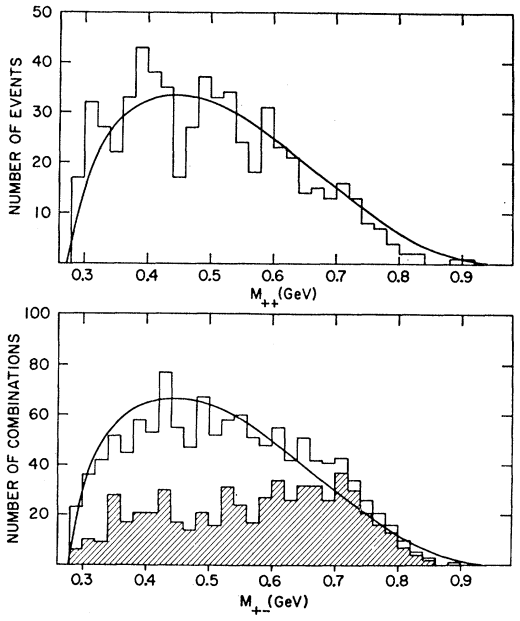

FIG. 22. Pion-pion effective-mass distributions from the reaction $\pi^+p \to \pi^+\pi^-\pi^+p$. The shaded events correspond to these $\pi^+\pi^-$ pairs in which the other π^+ is associated with the N*(1238) (620 events).

for the combinatorial background from the extra π^+ in this reaction, we conclude that the isobar N*(1238) in its $I_3=\frac{3}{2}$ substate is produced in almost every interaction. There is no indication of the $I_3=-\frac{1}{2}$ substate in the $p\pi^-$ effective-mass distribution.

Figure 22 shows the $\pi^+\pi^-$ and $\pi^+\pi^+$ effective-mass distributions. In the distribution of the $\pi^+\pi^-$ effective masses, those events in which the other π^+ is associated with $N^*(1238)$ have been shaded. While our center-of-mass energy is sufficient for the reaction

$$\begin{array}{ccc} \pi^+ + p \rightarrow N_{3/2}^* & & +\rho^0 \\ & \searrow & \searrow \\ & \pi^+ + p & \pi^+ + \pi^- \end{array} \qquad (4c)$$

to take place, there is only slight evidence for an accumulation of the shaded events in the ρ region of the $\pi^+\pi^-$ mass spectrum. Figure 23 shows the distribution of q^2, the square of the four-momentum transfer to the π^+p system, with events in the $N^*(1238)$ region shaded. We note that at our energy reaction (4c) would necessarily involve large values of q^2.

All departures from phase space of the three-body effective-mass distributions can be attributed to kinematic effects of $N^*(1238)$ decaying into $p\pi^+$.

Figure 24 shows histograms of the $n\pi^+$ and $n\pi^-$ effective masses from reaction (4b). The $n\pi^-$ plot is peaked at the low-energy end of the spectrum suggestive of $N^*(1238)$ formation, although the central mass is somewhat lower than the 1220 MeV usually observed for this resonance. The $n\pi^+$ distribution follows the phase-space curve

Thirty-two events of the type $\pi^+ + d \rightarrow \pi^+ + \pi^- + \pi^+ + d$ [reaction (5)], corresponding to a cross section of 0.080±0.016 mb, were separated from the events of reaction (4) on the basis of ionization and kinematic information. In 19 of these events there was a heavy stopping track which could not be identified visually as a deuteron but that interpretation was strongly favored in the kinematic fitting. Figure 25 shows the

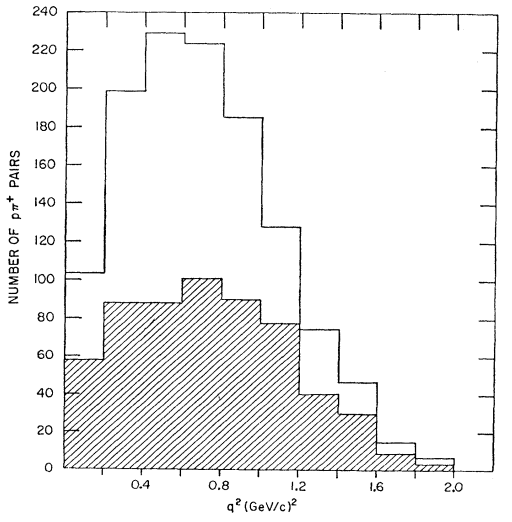

FIG. 23. Distribution of the square of the four-momentum transfer to the π^+p system for the reaction $\pi^+p \rightarrow \pi^+\pi^-\pi^+p$. Events associated with $N^*(1238)$ are shaded.

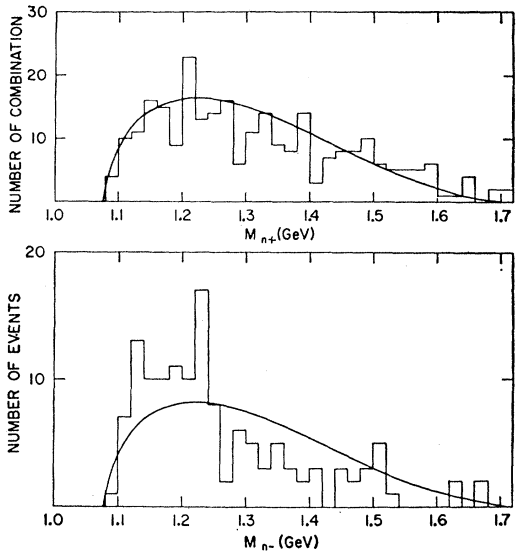

FIG. 24. Effective-mass distribution of the $n\pi^+$ and $n\pi^-$ systems from the reaction $\pi^+n \rightarrow \pi^+\pi^-\pi^+n$. The phase-space prediction is indicated by the curve (147 events).

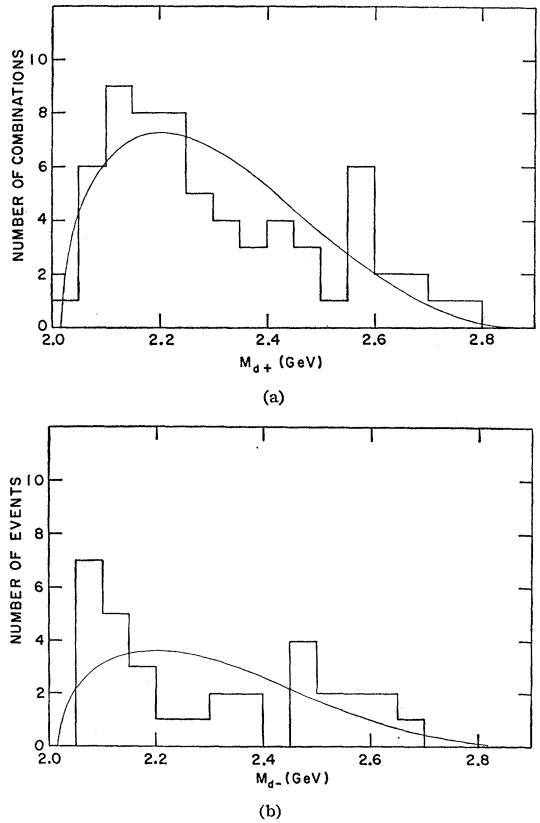

FIG. 25. Effective-mass distributions of $d\pi^+$ and $d\pi^-$ from the reaction $\pi^+d \rightarrow \pi^+\pi^-\pi^+d$. Phase space is indicated by the curves.

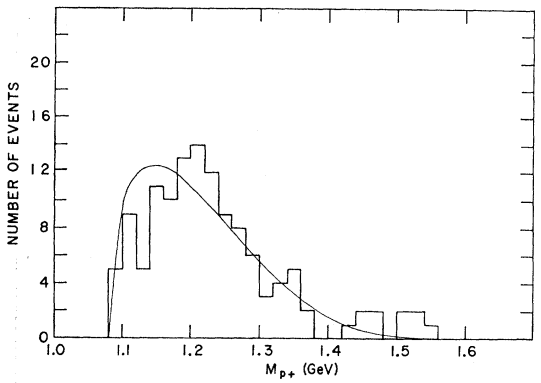

FIG. 26. Effective-mass distribution of the π^+p system from the reaction $\pi^+n \to 2\pi^+ + 2\pi^- + p$. Phase space is indicated by the curves.

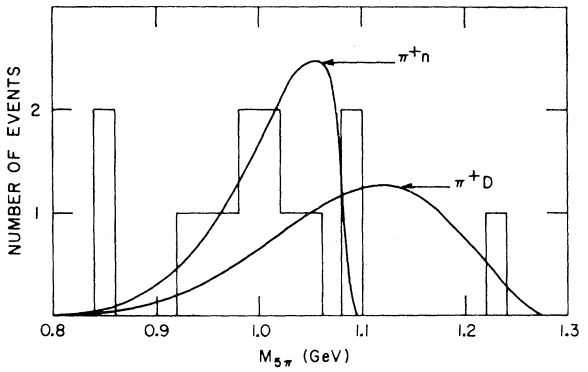

FIG. 27. Multipion effective-mass associated with the two protons in the reaction $\pi^+d \to \pi^+\pi^-\pi^+\pi^-\pi^0pp$. The curves show the phase-space predictions for interaction of the incident pion with the whole deuteron and with a free neutron (14 events).

$d\pi^+$ and $d\pi^-$ effective-mass distributions. Both distributions peak at low-mass values suggestive of the formation of the deuteron resonance observed in π^+d and π^-d interactions at higher energies.[32]

IX. THE REACTIONS $\pi^+d \to 2\pi^+ + 2\pi^- + 2p$ AND $\pi^+d \to 2\pi^+ + 2\pi^- + \pi^0 + 2p$

The reaction was studied by selecting events in which one proton behaves as a spectator ($P_p < 200$ MeV/c in the laboratory system),

$$\pi^+ + n \to 2\pi^+ + 2\pi^- + p. \tag{5a}$$

The cross section for this reaction is listed in Table I. Figure 26 shows the distribution of the $p\pi^+$ effective masses and indicates the dominance of $N^*(1238)$ in this reaction. There appear to be no other strong effects in the various mass distributions, but only very strong resonances could be observed above the heavy combinatorial background.

The events of reaction (6) cannot be fitted by our kinematics program because of the large number of particles in the final state. However, the missing mass for the reaction was calculated, and events consistent with production of a single π^0 were selected. The missing mass associated with the two protons was then calculated to give the five-pion mass plotted in Fig. 27. These few events provide an upper limit to the cross section for the reaction

$$\begin{array}{l} \pi^+ + d \to \eta^*(960) + p + p \\ \qquad\qquad \searrow \\ \qquad\qquad 2\pi^+ + 2\pi^- + \pi^0 \end{array} \tag{6a}$$

of 0.025 mb. We obtain this by considering the nine events near 1 GeV as the maximum number of candidates for the reaction.

ACKNOWLEDGMENTS

We would like to thank the operating crews of the AGS, the separated beam, and the 20-in. bubble chamber, and our scanning and measuring staff for their cooperation. We are indebted to Professor J. D. Jackson, Professor Y. T. Chiu, Professor F. Selleri, and Professor M. Barmawi for their comments and discussions of our data.

[32] M. A. Abolins, D. D. Carmony, R. L. Lander, and Ng. h. Xuong, Phys. Letters **15**, 125 (1965). Saclay-Orsay-Bari-Bologna-Firenze Collaboration, *ibid.* **19**, 68 (1965). G. Vegni, H. Winzeler, P. Zaniol, P. Fleury, and G. DeRosny, *ibid* **19**, 426 (1965).